Variable porosity and thermal dispersion effects on coupled heat and mass transfer by natural convection from a surface embedded in a non-metallic porous medium

Received April 2000
Revised February 2001
Accepted February 2001

Abdul-Rahim A. Khaled and Ali J. Chamkha
Department of Mechanical and Industrial Engineering, Kuwait University, Safat, Kuwait

Keywords *Variable porosity, Thermal dispersion, Heat transfer, Porous medium, Natural convection*

Abstract *The problem of coupled heat and mass transfer by natural convection from a vertical impermeable semi-finite flat plate embedded in a non-uniform non-metallic porous medium in the presence of thermal dispersion effects is formulated. The plate surface is maintained at constant wall temperature and concentration. The resulting governing equations are non-dimensionalized and transformed using a non-similarity transformation and then solved numerically by an implicit, iterative, finite-difference scheme. A parametric study of all involved parameters is conducted and a representative set of numerical results is illustrated graphically to show typical trends of the solutions. It is found that the variable porosity of the porous medium and the effect of thermal dispersion result in increases in the local Nusselt number.*

Nomenclature

C = concentration at any point in the field
C_o = concentration at the wall
C_∞ = concentration at the free stream
c = dimensionless concentration
c_p = fluid specific heat at constant pressure
D = mass diffusivity
d_p = diameter of the porous medium particles
e = buoyancy ratio
F = inertia coefficient of the porous medium
f = dimensionless stream function
g = gravitational acceleration
h = local convection heat transfer coefficient
h_m = local mass transfer coefficient
K = permeability of the porous medium
k_e = effective thermal conductivity of the porous medium
k_f = thermal conductivity of the pure fluid
k_d = thermal conductivity of the porous medium material
L = characteristic length of the plate
Le = Lewis number
Nu = local Nusselt number
Nu_{AVG} = average Nusselt number
Pr = Prandtl number
R = dimensionless temperature
R_o = dimensionless (normalized) wall temperature
Sh_x = local Sherwood number
Sh_{AVG} = average Sherwood number
SFP = local skin-friction parameter

International Journal of Numerical Methods for Heat & Fluid Flow, Vol. 11 No. 5, 2001, pp. 413-429.

SFP_{AVG} = average skin-friction parameter
T = temperature at any point
T_o = wall temperature
T_∞ = free stream temperature
U = tangential velocity
u = dimensionless tangential velocity
V = normal velocity
v = dimensionless normal velocity
X = distance along the plate
x = dimensionless distance along the plate
Y = distance normal to the plate
y = dimensionless distance normal to the plate

Greek symbols
α_e = effective thermal diffusivity of the porous medium
α_s = free stream effective thermal diffusivity of the porous medium
β_c = concentration expansion coefficient
β_T = thermal expansion coefficient
ζ = transformed concentration
η = coordinate transformation in terms of x and y
ε = porosity of the porous medium
ε_s = free stream porosity of the porous medium
μ = dynamic viscosity
υ = kinematic viscosity
Ψ = stream function
θ = transformed temperature
τ_w = wall shear stress
ρ = fluid density
ξ = coordinate transformation for x

Introduction

Coupled heat and mass transfer in fluid-saturated porous media is a subject that attracted the interest of many investigators. This interest stems from its application in a variety of engineering processes such as heat exchangers, insulation systems, petroleum reservoirs, chemical catalytic reactors and processes, and nuclear waste repositories. There has been considerable work done on the study of flow and heat transfer in geometries with and without porous media (see, for instance, Churchill and Chu, 1975; Vafai and Tien, 1981).

Early work on porous media modeling has used the linear Darcy law extensively. For example, the problem of natural convection in a porous medium supported by an isothermal vertical plate was solved some time ago by Cheng and Minkowycz (1977) using the Darcy law. It is well established now that the Darcy law is inapplicable for high velocity flow situations for which the relation between the pressure drop and the Darcian velocity is nonlinear, and that it does not account for the presence of a boundary at which the no-slip condition must be satisfied. Johnson and Cheng (1978), Vafai and Tien (1981) and Plumb and Huenefeld (1981) considered inertia and boundary effects in porous media. Recently, Kou and Huang (1996) have developed non-similar transformations for natural convection flow along a vertical plate embedded in a porous medium with a prescribed temperature condition.

Inspite of its performance in many processes, the problem of coupled heat and mass transfer has received relatively little attention. Bejan and Khair (1985) reported on the natural convection boundary-layer flow in a saturated porous medium with combined heat and mass transfer. The coupled heat and mass buoyancy-induced boundary layer in a porous medium was studied by Jang and Chang (1988). Trevisan and Bejan (1990) considered combined heat and mass transfer by natural convection in a porous medium for various geometries. Later, Lai and Kulacki (1991) have extended the problem of Bejan and Khair (1985) to include wall fluid injection effects. Early studies which

considered coupled heat and mass transfer without the presence of porous media include the works of Gebhart and Pera (1971) on vertical plates, and Pera and Gebhart (1972). Recently, Lai (1991) and Yih (1997) have studied coupled heat and mass transfer by mixed convection from a vertical plate embedded in a fluid-saturated porous medium.

Most realistic porous media have variable permeability and inertia coefficient. The variations in these parameters are due to the fact that the porosity distributions of these media are not uniform; particularly in packed beds of spheres. In their experiments, Benenati and Brosilow (1962) have shown a distinct porosity variation with a high porosity region close to the solid wall in packed beds. The study of variable porosity in porous media modeling has been developing at the same time with the study of thermal dispersion (better explained by Cheng, 1981; Plumb, 1983; and Amiri and Vafai, 1994). Hong and Tien (1987) have analyzed the problem of thermal dispersion effects on natural convection about a heated horizontal cylinder in an enclosed porous medium. Hsiao *et al.* (1992) have discussed the effects of non-uniform porosity and thermal dispersion on natural convection about a heated horizontal cylinder in an enclosed porous medium. Hsiao *et al.* (1992) have shown that including the effects of variable porosity and thermal dispersion increases the average Nusselt number and reduces the error between the experimental data available and their solutions. It should be noted here that, to the best of the authors' knowledge, no experimental data appear to be available for natural convection over a vertical plate embedded in a porous medium in order to compare with the work in this paper. Also, there is no work done on combined heat and mass transfer over a vertical plate by natural convection embedded in a porous medium with a variable porosity distribution and thermal dispersion effects. This is the purpose of the present work.

Problem formulation

Consider steady, laminar heat and mass transfer by natural convection flow along an impermeable semi-infinite vertical plate embedded in a fluid-saturated non-uniform non-metallic porous medium taking into account the effects of thermal dispersion of the porous medium. The surface of the plate is maintained at constant temperature and concentration. Both the temperature and concentration at the plate are always greater than their uniform ambient values existing far from the plate surface. The fluid is assumed to be Newtonian, viscous, and has constant properties except the density in the buoyancy term of the balance of momentum equation. Invoking the Boussinesq and boundary layer approximations, the governing equations for this problem can be written as

$$\frac{\partial \mathrm{U}}{\partial \mathrm{X}} + \frac{\partial \mathrm{V}}{\partial \mathrm{Y}} = 0 \tag{1}$$

$$U\frac{\partial U}{\partial X}+V\frac{\partial U}{\partial Y}=\upsilon\frac{\partial^2 U}{\partial Y^2}+\beta_T g(T-T_\infty)+\beta_c g(C-C_\infty)-\frac{\upsilon\varepsilon}{K}U-F\varepsilon^2U^2 \quad (2)$$

$$U\frac{\partial T}{\partial X}+V\frac{\partial T}{\partial Y}=\frac{\partial}{\partial Y}(\alpha_e\frac{\partial T}{\partial Y}) \quad (3)$$

$$U\frac{\partial C}{\partial X}+V\frac{\partial C}{\partial Y}=D\frac{\partial^2 C}{\partial Y^2} \quad (4)$$

where U, V, T and C are the fluid x-component of velocity, y-component of velocity, temperature, and concentration, respectively. ρ, υ, β_T, and β_c are the fluid density, kinematic viscosity, coefficient of thermal expansion, and coefficient of concentration expansion, respectively. D and g are the mass diffusivity and the gravitational acceleration, respectively. ε, K, F, and α_e are the porous medium porosity, permeability, inertia coefficient, and effective thermal diffusivity, respectively. T_∞ and C_∞ are the ambient fluid temperature and concentration, respectively.

Based on the experimental results on porosity distribution in packed beds obtained by Benenati and Brosilow (1962), Amiri and Vafai (1994) have shown that the porosity can be expressed by the following exponential relationship:

$$\varepsilon=\varepsilon_s(1+a_1\exp(\frac{-a_2Y}{d_p})) \quad (5)$$

where ε_s is the free-stream porosity, d_p is the particle diameter, and a_1 and a_2 are empirical constants which depend on the ratio of the bed to particle diameter and are determined experimentally. Amiri and Vafai (1994) suggested 0.37, 1.7 and 6.0 for the values of ε_s, a_1 and a_2, respectively. These values were found to best fit the experimental data collected by Roblee *et al.* (1958) and Benenati and Brosilow (1962). The permeability and the inertia coefficient are given by

$$K(Y)=\frac{d_p^2\varepsilon^3}{150(1-\varepsilon)^2} \quad (6)$$

$$F(Y)=\frac{1.75(1-\varepsilon)}{\varepsilon^{9/4}d_p} \quad (7)$$

Amiri and Vafai (1994) have employed the following relation for the effective thermal conductivity k_e which represents the sum of the molecular thermal conductivity (the first term) and the thermal conductivity due to dispersion (the second term):

$$k_e = (\varepsilon + 0.1[\Pr(\frac{\rho u d_p}{\mu})])k_f + (1-\varepsilon)k_d \tag{8}$$

where k_f and k_d are the fluid molecular and the porous medium material thermal conductivities, u is the dimensionless tangential velocity, μ is the dynamic viscosity of the fluid and Pr ($=\mu c_p/(\varepsilon_s K_f)$) is the Prandtl number.

Non-dimensionalization of the above equations is obtained by using

$$\begin{aligned} x &= \frac{X}{L}, \quad y = \frac{Y}{L}, \quad u = \frac{UL}{\alpha_s}, \quad v = \frac{VL}{\alpha_s}, \\ R &= \frac{T - T_\infty}{\alpha_s \upsilon/(g\,\beta_T\,L^3)}, \quad c = \frac{C - C_\infty}{\alpha_s \upsilon/(g\,\beta_c\,L^3)} \end{aligned} \tag{9}$$

where L and α_s ($\alpha_s =_s k_f/(\rho c_p)$) are, respectively, characteristics of plate length and the molecular thermal diffusivity at the free stream. Using the following non-similarity transformations reported earlier by Kou and Huang (1996):

$$\eta = \frac{R_o^{1/4}}{x^{1/4}}, \quad \xi = x, \quad f(\xi,\eta) = \frac{\psi(x,y)}{R_o^{1/4}\,x^{3/4}}, \quad \theta(\xi,\eta) = \frac{R(x,y)}{R_o} \tag{10}$$

where $R_o(= g\beta_T(T_o - T_\infty)L^3/\upsilon)$ is the dimensionless wall temperature (or Rayleigh number), defining

$$\varsigma = \frac{c(x,y)}{c_o} \quad \text{and} \quad e = \frac{\beta_c\,(C_o - C_\infty)}{\beta_T\,(T_o - T_\infty)} \tag{11}$$

where $c_o(= g\beta_T(C_o - C_\infty)L^3/\upsilon), T_o, C_o$, and e are the dimensionless concentration at the wall, the wall temperature and concentration and the buoyancy ratio which is the ratio of the buoyancy forces due to concentration change to the buoyancy forces due to temperature change, respectively and then substituting equations (10) and (11) into the non-dimensionalized from of equations (2) through (4) yields the following non-similar equations:

$$\begin{aligned} f''' + \frac{1}{\Pr}[\frac{3}{4}ff'' - \frac{1}{2}(f')^2 - \xi(f'\frac{\partial f'}{\partial \xi} - f''\frac{\partial f}{\partial \xi})] + \theta + e\varsigma &= \frac{150(1-\varepsilon)^2 L^2}{d_p^2 \varepsilon^3 R_o^{1/2}}\xi^{1/2} f' \\ &\quad + \frac{1.75(1-\varepsilon)L}{d_p\ \Pr\ \varepsilon^{1/4}}\xi(f')^2 \end{aligned} \tag{12}$$

$$\frac{k_e}{k_s}\theta'' + \frac{1}{k_s}(\frac{\partial k_e}{\partial \eta})\theta + \frac{3}{4}f\,\theta' = \xi\,(f'\frac{\partial \theta}{\partial \xi} - \theta'\frac{\partial f}{\partial \xi}) \tag{13}$$

$$\frac{1}{\mathrm{Le}}\varsigma'' + \frac{3}{4}\mathrm{f}\varsigma' = \xi(\mathrm{f}'\frac{\partial \varsigma}{\partial \xi} - \varsigma'\frac{\partial \mathrm{f}}{\partial \xi}) \tag{14}$$

where a prime denotes differentiation with respect to η and $k_s(=\varepsilon_s k_f)$ and Le $(=\alpha_s / D)$ are the molecular conductivity at the free stream and Lewis number, respectively, and

$$\varepsilon = \varepsilon_s(1 + a_1 \exp(\frac{-a_2 L\xi^{1/4}\eta}{d_p R_o^{1/4}})) \tag{15}$$

It should be noted here that the porous medium is assumed to be nonmetallic (glass fibers), such that $k_d << k_f$ and, therefore, the last term of equation (8) is neglected. The dimensionless boundary conditions for this problem can be written as

$$\begin{array}{lll} U(X,0) = 0, & U(X,\infty) = 0, & V(X,0) = 0, \\ T(X,0) = T_o, & T(X,\infty) = T_\infty, & C(X,0) = C_o, \quad C(X,\infty) = C_\infty \end{array} \tag{16}$$

The transformed dimensionless boundary conditions become

$$\begin{array}{lll} f'(\xi,0) = 0, & f'(\xi,\infty) = 0, & f(\xi,0) = 0, \\ \theta(\xi,0) = 1, & \theta(\xi,\infty) = 0, & \varsigma(\xi,0) = 1, \quad \varsigma(\xi,\infty) = 0 \end{array} \tag{17}$$

Of special interest for this flow and heat transfer situation are the skin-friction parameter, Nusselt number, and the Sherwood number. These are defined as follows

$$\mathrm{SFP} = \frac{\tau_w}{\mu(L^2/\alpha_e)R_o^{3/4}} = \xi^{3/4} f''(\xi,0), \quad \mathrm{SFP_{AVG}} = \frac{\int (\mathrm{SFP})\,dx}{\int dx} \tag{18}$$

$$\mathrm{Nu} = \frac{hx}{k_s} = -\xi^{3/4} R_o^{1/4}\theta'(\xi,0), \quad \mathrm{Nu_{AVG}} = \frac{L}{k_s}\,\frac{\int h dx}{\int dx} \tag{19}$$

$$\mathrm{Sh_x} = \frac{h_m x}{D} = -\xi^{3/4} R_o^{1/4}\varsigma'(\xi,0), \quad \mathrm{Sh_{AVG}} = \frac{L}{D}\,\frac{\int h_m dx}{\int dx} \tag{20}$$

where τ_w, h and h_m are the shear stress at the wall, convective heat transfer coefficient and the local mass transfer coefficient, respectively, and $\mathrm{SFP_{AVG}}$, $\mathrm{Nu_{AVG}}$ and $\mathrm{Sh_{AVG}}$ are the average skin-friction parameter, Nusselt number and Sherwood number, respectively.

Numerical method

The resulting non-similar equations (equations (12) through (14)) for the problem are nonlinear and must be solved numerically with iteration subject to the corresponding boundary conditions. The implicit finite-difference method

discussed by Blottner (1970) has proven to be accurate for the solution of such equations. The method starts with a change of variable such that $V = f'$ in order to reduce the momentum equation (12) into a second-order non-similar differential equation. Then, the equations governing V, θ, and ζ are discretized using three-point central different quotients and are arranged in a tri-diagonal system of algebraic equations that can be solved by the well-known Thomas algorithm. But, due to the nonlinearities of the equations, an iterative solution is expected. The solution marches from $\xi = 0$ to $\xi = 1$ using a two-point backward difference formula in the ξ direction. A variable step size in the ν direction is selected since rapid changes in the dependent variables are expected near the wall. With a starting step size in the η direction of 0.001 at the wall and a step size growth factor of 1.03 such that $\Delta\eta_{n+1} = 1.03\Delta\eta_n$ accurate results can be obtained with minimum computational efforts. Moreover, a constant step of 0.05 in the ξ direction was selected after performing many trials to assess grid independence. The convergence criterion for this problem required that the difference between the current and the previous iterations be 10^{-8}. Once the solutions for V, θ, and ζ are converged, the equation $V = f'$ is solved for by the trapezoidal rule.

It should be mentioned here that the above numerical method was employed to solve the non-similar equations in the absence of the porous medium and ignoring the mass diffusion equation. The results of f', θ and Nu for this case were found to be in excellent agreement with the solution of laminar natural convection boundary layer flow along an isothermal vertical wall reported by Bejan (1993). This comparison lends confidence in the adequacy and accuracy of the numerical method.

Results and discussion

Figures 1 and 2 present the behavior of the induced tangential velocity and dimensionless temperature profiles at $\xi = 1$ for various values of the porosity

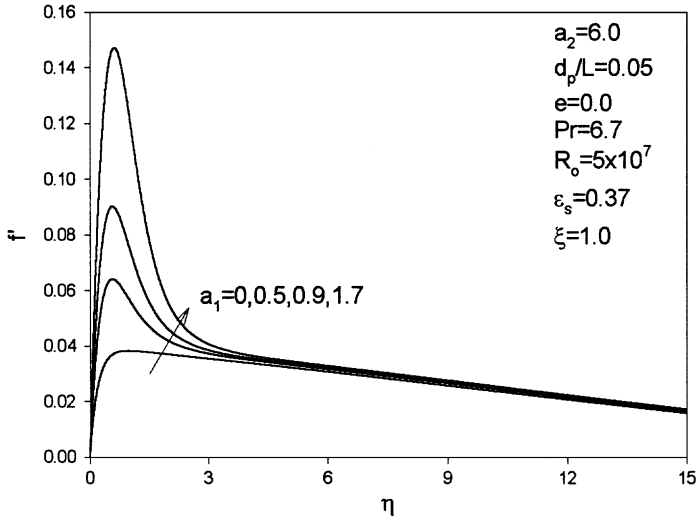

Figure 1.
Effects of a_1 on tangential velocity profiles

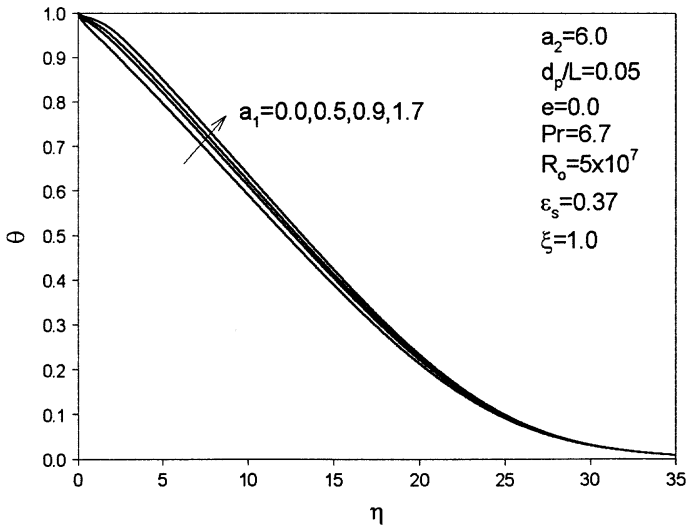

Figure 2.
Effects of a_1 on temperature profiles

distribution parameter a_1, respectively. In all of the figures to be reported subsequently unless otherwise stated, the reference values of the parameters a_1, a_2, d_p/L, Pr, R_o and ε_s are 1.7, 6.0, 0.05, 6.7, 5×10^7 and 0.37, respectively and the other parameters are set to zero. It is seen that increasing a_1 not only results in a decrease in the tightness of the porous medium but it also results in an increase in the thermal diffusivities at and near the wall due to the presence of large porosities in this region for the variable porosity model compared to the reference case where the porosity is constant. Notice that for large values of η, the transformed dimensionless tangential velocity f′ for all values of a_1 will have the same value which means that the porosity reaches its constant value where the velocity does not reach the free-stream value. It is interesting to notice the existence of the peaks in the velocity profiles in the region close to the wall. This type of behavior is called the channelling effect and has been reported earlier by many previous investigators (see, for instance, Vafai and Tien, 1981). The increase in the flow temperature is expected because of the increased thermal conductivity as a_1 increases. This increase in the thermal conductivity and the enhanced flow velocity require increases in the wall heat flux to maintain energy conservation.

Figures 3 and 4 illustrate the trends of the local skin-friction parameter and the local Nusselt number distribution along the surface for different values of a_1, respectively. Since the induced tangential velocity increases as a_1 increases, its slope at the wall increases. Therefore, the skin-friction parameter increases as a1 increases as shown in Figure 3. The definition of the local Nusselt number in Figure 4 is based on the effective thermal conductivity of the porous medium at the wall makes the comparison between the curves according to their dimensionless convective heat transfer coefficient difficult because of the difference in porosities at the wall. Defining $Nu_m(Nu_m = Nu(k_o/k_s))$ as the

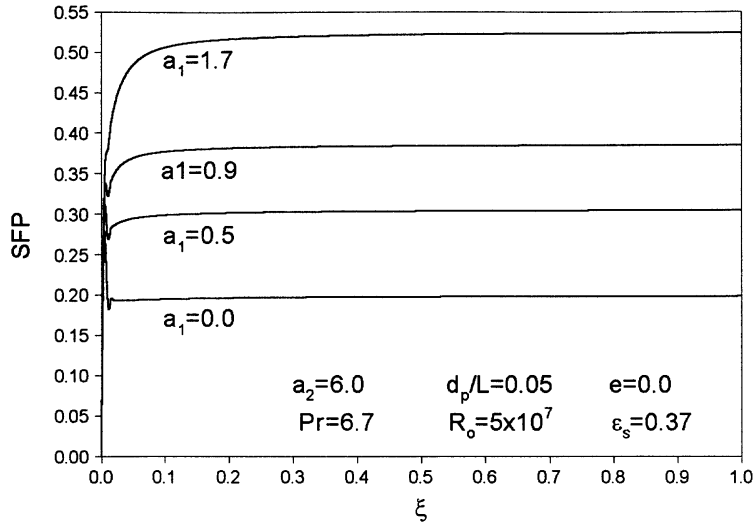

Figure 3.
Effects of a_1 on the skin-friction parameter

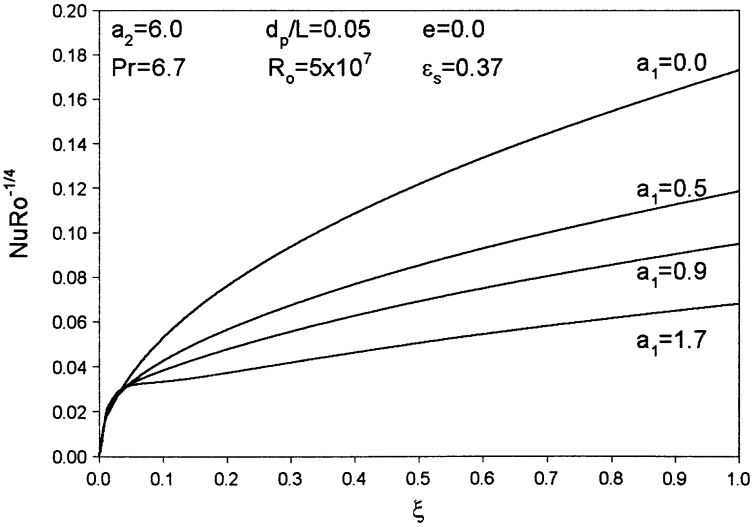

Figure 4.
Effects of a_1 on the local Nusselt number

equivalent dimensionless local heat convective transfer coefficient as if the thermal conductivity is constant at the free stream condition k_s for all the cases, provided similar porosity and liquid properties at the free stream region exist. Therefore, the values of Nu_m increase as a_1 increases and this can be detected from Figure 4. Notice that the skin-friction parameter is higher for the case where the thermal dispertion is neglected where as the local Nusselt number is higher as shown from Figures 3 and 4, respectively.

Figures 5 and 6 illustrate the behavior of the induced tangential velocity and the dimensionless temperature at $\xi = 1$ for different values of the ratio d_p/L for a uniform wall temperature condition, respectively. For large values of d_p/L, ε

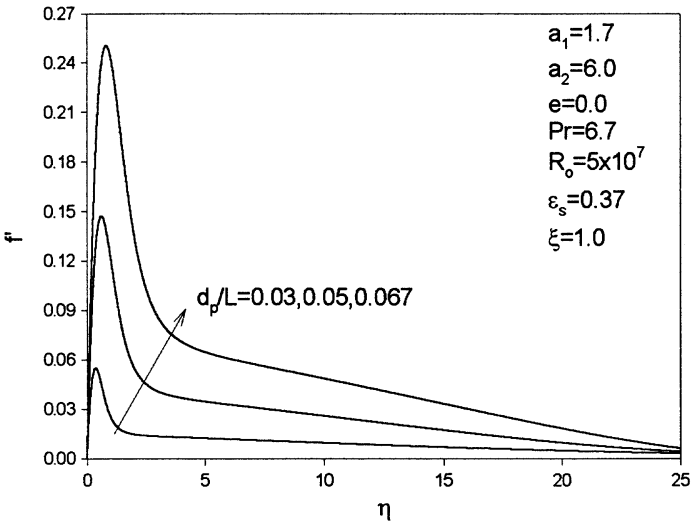

Figure 5.
Effects of d_p/L on tangential velocity profiles

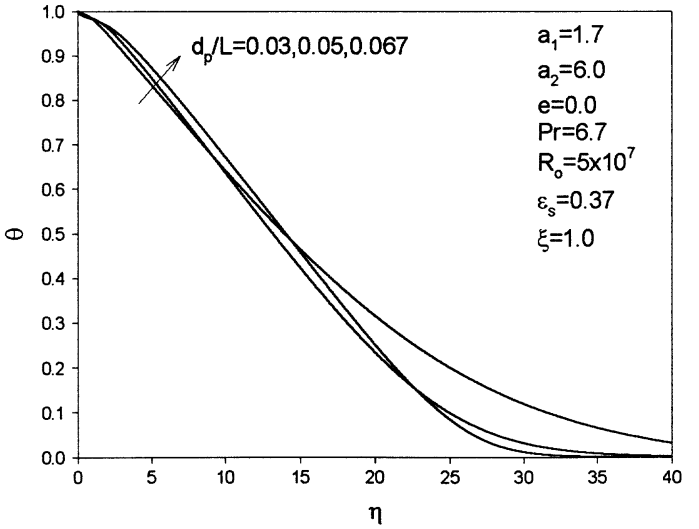

Figure 6.
Effects of a_1 on temperature profiles

reaches its free stream value after a larger distance compared to smaller values of d_p/L. Thus, as d_p/L increases, the voids volume increases causing the resistance against the flow to decrease which results in an increase in the induced tangential velocity. This is not the only reason since thermal diffusivities within the boundary layer increase due to increased porosity and thermal dispersion as d_p/L increases. Figure 5 is illustrative of these factors. The increase in the porosity as d_p/L increases results in increasing the convective thermal energy transfer due to the increase in the buoyancy forces compared to the thermal diffusion from the wall because all of the studied cases have the same effective thermal diffusivity at the wall. Thus, the flow

temperature (especially near the wall) decreases and the absolute slope of wall temperature increases as d_p/L increases. Notice that because of the large thermal dispersion near the wall, the temperature gradients there increase as d_p/L increases. These facts can be seen from Figure 6.

Figures 7 and 8 show the development of the local skin-friction parameter and the local Nusselt number along the surface for different values of d_p/L, respectively. The increase in the induced velocity and its slope near the wall at higher d_p/L values cause the local skin-friction parameter to increase as shown in Figure 7. As d_p/L increases, the convective thermal energy increases due to the increase in the thermal diffusion resulting from the increase in the thermal

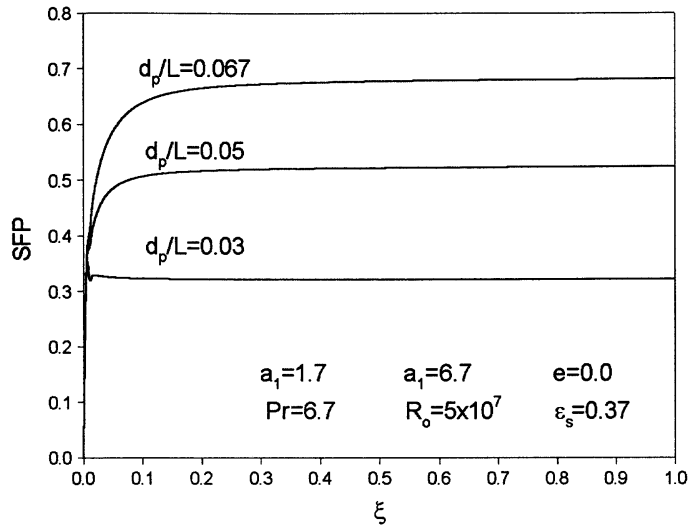

Figure 7.
Effects of d_p/L on the skin-friction parameter

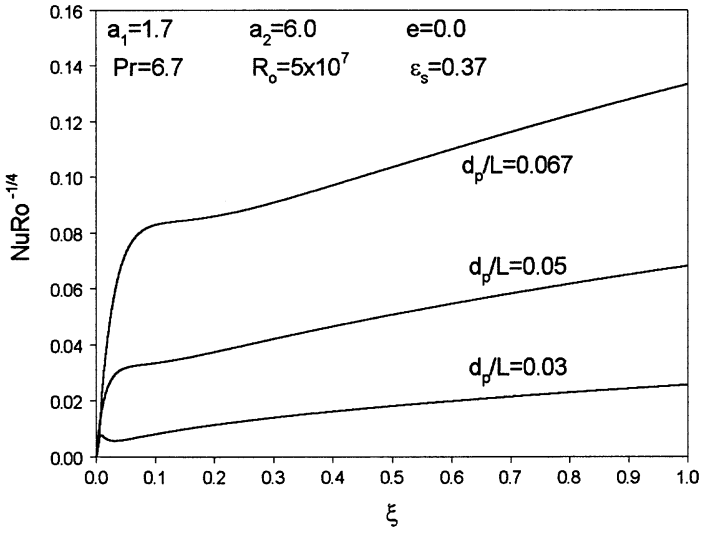

Figure 8.
Effects of d_p/L on the local Nusselt number

dispersion and the porosity near the wall. This results in increasing the wall heat flux removal. As a result, the Nusselt number increases with increases in the values of d_p/L as shown in Figure 8. The same can be said regarding the convective heat transfer coefficient and Nu_m.

Figures 9 and 10 illustrate the behavior of the induced tangential velocity and the dimensionless temperature at $\xi = 1$ for various values of dimensionless wall temperature R_o. The normal distances from the plate of any two points on these figures decrease as R_o increases. Thus, large changes in the porosity will be felt far away from the wall when R_o increases. Physically, this means that the boundary-layer thickness is expected to decrease as R_o increases such that

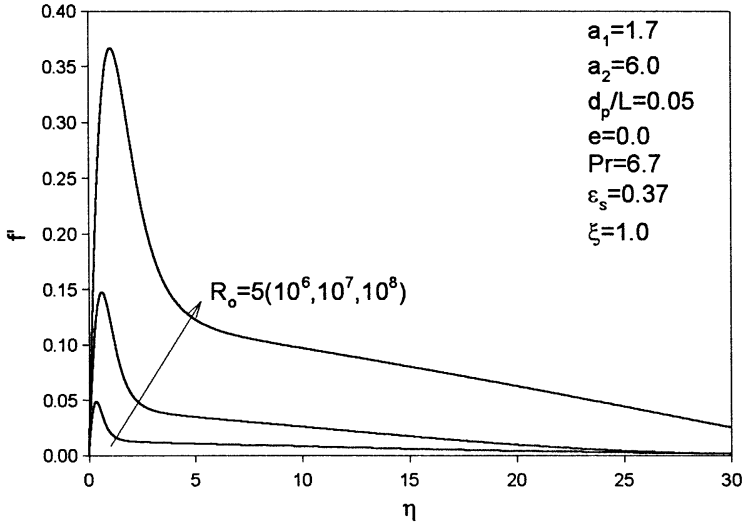

Figure 9.
Effects of R_o on tangential velocity profiles

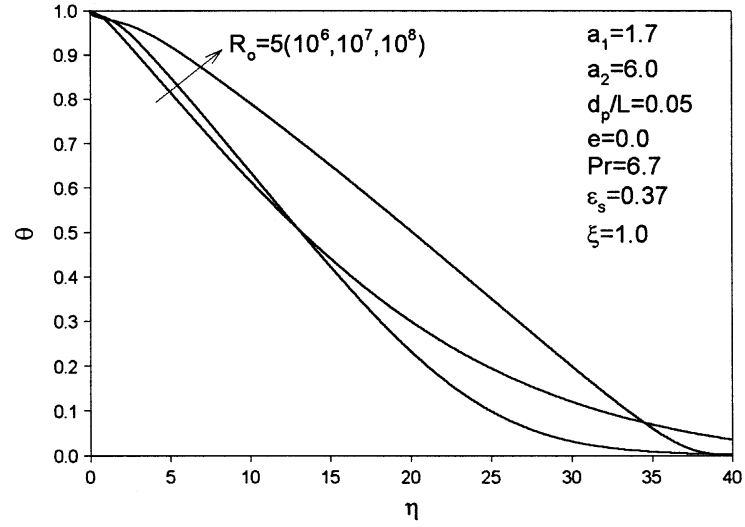

Figure 10.
Effects of R_o on temperature profiles

the free stream porosity is quite far from the porosity near the wall. Note that the normal distance, induced tangential velocity and the dimensionless temperature are not only functions of η, f′, and θ, respectively, but they are also functions of R_o where all of them except the normal distance increase as R_o increases. Similar to the effect of increasing the ratio d_p/L, is the fact that the coefficient A which is a measure of the tightness of the porous medium decreases as R_o increases, increasing Ro results in an increase in the induced velocity as shown in Figure 9. Also, this results in large thermal diffusion near the wall due to increases in both the porosity and thermal dispersion. Moreover, the increased speeds of the streamlines are capable of convecting the conducted wall heat flux from the wall at larger values of R_o compared to smaller ones. Accordingly, the absolute slope of the wall temperature increases and the flow temperature decreases as R_o increases as shown in Figure 10.

Figures 11 and 12 illustrate the behavior of the local skin-friction parameter and the local Nusselt number for different values of R_o, respectively. The increase in the induced velocity and its slope near the wall at higher values of R_o cause the local skin-friction parameter to increase as shown in Figure 11. It should be mentioned here that the wall shear stress is proportional to (SFP) $R_o^{3/4}$. In addition, as R_o increases, the flow velocity and thermal diffusion increase as a result of the variable porosity and dispersion effects causing a rapid increase in the rate of wall heat transfer. This, in turn, increases the local Nusselt number as shown in Figure 12. Similar trends are obtained for the convective heat transfer coefficient and Nu_m.

Figures 13-15 illustrate the effect of the buoyancy ratio e on the average skin-friction parameter SFP_{AVG}, the average fluid Nusselt number Nu_f and the average Sherwood number Sh_{AVG}, respectively. In these figures, the average skin-friction parameter increases for all the cases and a rapid increase is

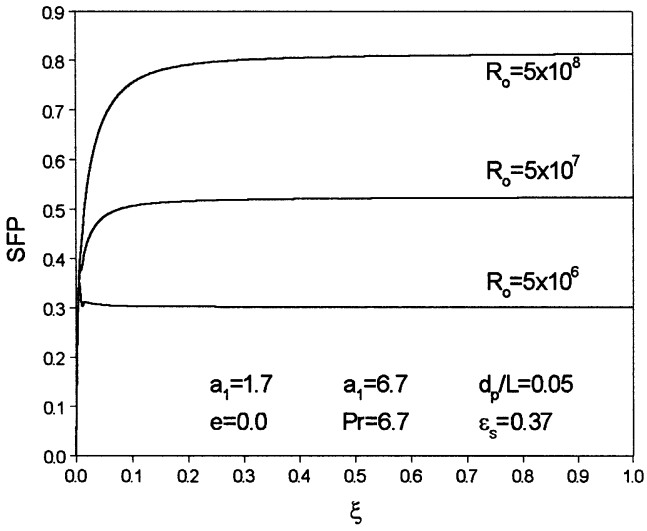

Figure 11.
Effects of R_o on the skin-friction parameter

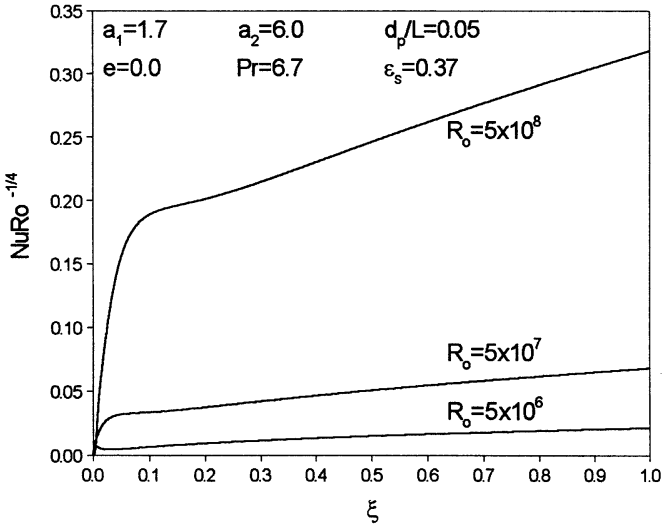

Figure 12.
Effects of R_o on the local Nusselt number

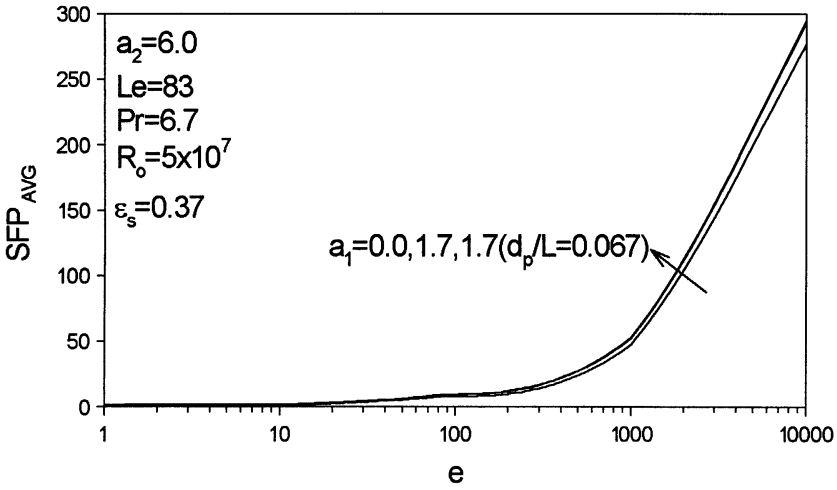

Figure 13.
Effects of e on the average skin friction parameter

noticed after e = 300. The total volume of voids is the smallest for the case where $a_1 = 0.0$ is the smallest for all values of e. By doing a scale analysis on laminar natural mass diffusion over a vertical plate similar to the scale analysis done by Bejan (1993) on laminar natural convection over a vertical plate, it is concluded that the concentration boundary-layer thickness decreases as the local Rayleigh number driven by mass (or local dimensionless concentration at the wall) increases.

Physically speaking, increasing e results in increases in the local dimensionless concentration at the wall. For the case of $d_p/L = 0.067$, the increase in the thermal diffusivity due to the variable porosity and thermal dispersion effects (due to increases in the buoyancy forces and also with the

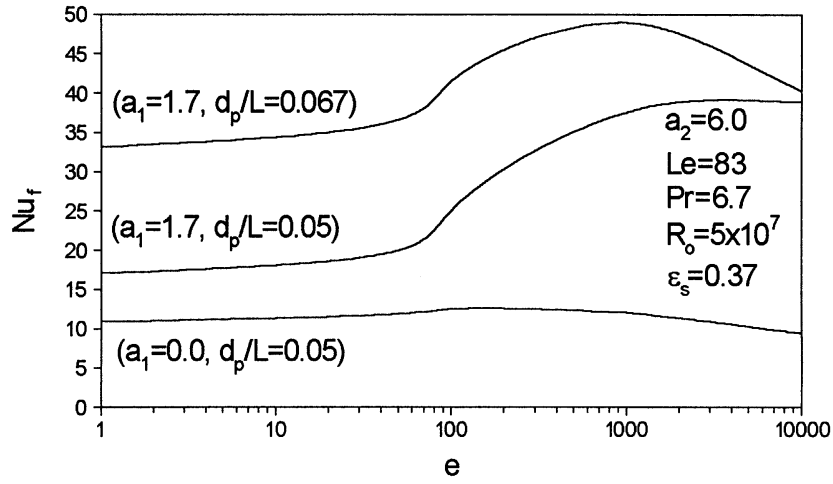

Figure 14.
Effects of e on the average fluid Nusselt number

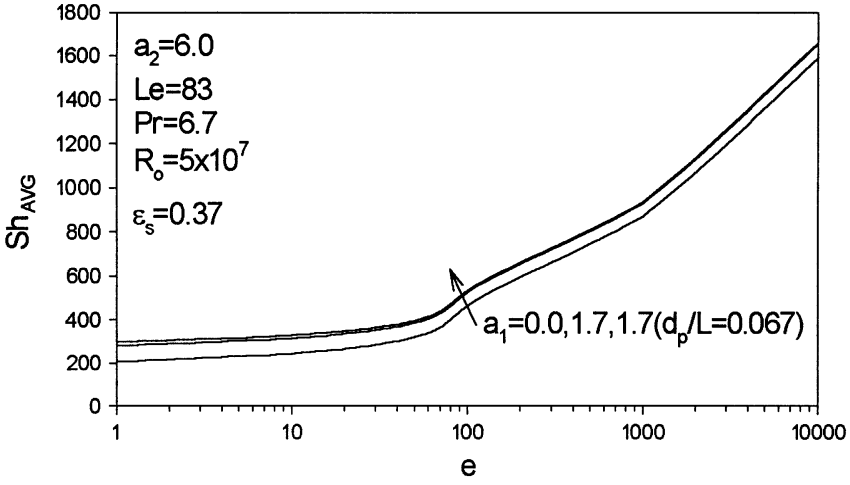

Figure 15.
Effects of e on the average Sherwood number

help of increases in the average flow velocity) causes the values of Nu_f to increase. But when e increases further, the maximum induced velocity moves closer to the wall (channeling effect) and the resistance due to the porous medium inertia effects will increase rapidly (since it is a function of u^2) causing a relative decrease in the induced velocity and, thus, a decrease in thermal dispersion despite the fact that the maximum thermal dispersion occurs in the region of maximum porosity. This results in decreasing the effective thermal diffusivity compared to cases of lower e values where the maximum Nu_f values occur. This, in turn, results in decreasing the amount of heat convected by the enthalpy streams as can be seen from Figure 14 after e = 1,000. For $d_p/L = 0.05$, the values of Nu_f are lower due to lower thermal dispersion effects and the point of maximum Nu_f value is shifted to the right since the porosity thickness is

reduced due to lower particle diameter which requires a large value of e to bring maximum induced velocities near the region of variable porosity.

The case of $a_1 = 0.0$ has the lowest Nu_f value because it has the minimum porosity. Hence, it has the minimum effective thermal conductivity over the whole domain. For a constant porosity model, the maximum Nu_f value occurs at e = 100. Actually, the reason is also associated with the decrease in the thermal dispersion as the induced velocity increases at large values of e because of the porous medium inertia effects as they are greater in this case than in the other cases. This allows an earlier response to the porous medium inertia effects for this case as e increases. Thus, Nu_f is expected to decrease at higher values of e and the optimum one is found at e =100 as shown in Figure 14.

In Figure 15, it is noticed that the average Sherwood number increases as e increases and that it is highest for the value of e with the highest porosity which is for $a_1 = 1.7$ and $d_p/L = 0.067$. The increase in the value of Sh_{AVG} becomes greater after e = 80. This is associated with high Lewis numbers which make the mass diffusivity small. Thus, relatively higher mass buoyancy ratios are needed to initiate the flow and, hence, to extract mass from the wall.

Conclusion

The problem of steady, laminar coupled heat and mass buoyancy-induced natural convection boundary-layer flow of Newtonian fluid along an isothermal vertical semi-infinite surface embedded in a non-uniform porous medium was considered. The governing equations were developed and transformed using appropriate non-similarity transformations. The transformed equations were then solved numerically by an implicit, iterative, finite-difference scheme. The obtained results for special cases of the problem were compared with previously published work and found to be in excellent agreement. It was found that the skin-friction parameter and the Nusselt number were increased as a result of the presence of variable porosity and thermal dispersion effects. Also, they increased when the particle diameter of the porous medium and the reference dimensionless wall temperature were increased where the Nusselt number was found to be higher than the case of a pure fluid for a large reference wall temperature. Eventually, it was found that the increase in the buoyancy ratio increased the skin-friction coefficient and the Sherwood number but the last statement was not always true for the Nusselt number. It is hoped that the present work will serve as a vehicle for understanding more complex problems involving variable porosity and thermal dispersion effects.

References

Amiri, A. and Vafai, K. (1994), "Analysis of dispersion effects and non-thermal equilibrium, non-Darcian, variable porosity incompressible flow through porous media", *Int. J. Heat Mass Transfer*, Vol. 37, pp. 939-54.

Bejan, A. (1993), *Convection Heat Transfer*, 2nd ed., Wiley, New York, NY, p. 176.

Bejan, A. and Khair, K.R. (1985), "Heat and mass transfer by natural convection in a porous medium", *Int. Commun. Heat Mass Transfer*, Vol. 28, pp. 909-18.

Benenati, R.F. and Brosilow, C.B. (1962), "Void fraction distribution in a bed of spheres", *A.I.Ch.E. J.*, Vol. 8, pp. 361-95.

Blottner, F.G. (1970), "Finite-difference methods of solution of the boundary-layer equations", *AIAA Journal*, Vol. 8, pp. 193-205.

Cheng, P. (1981), "Thermal dispersion effects in non-darcian convective flows in a saturated porous medium", *Lett. Heat Mass Transfer*, Vol. 8, pp. 267-70.

Cheng, P. and Minkowycz, W.J. (1977), "Free convection about a vertical flat plate embedded in a porous medium with application to heat transfer from a dike", *J. of Geophy. Res.*, Vol. 82, pp. 2040-4.

Churchill, S.W. and Chu, H.H.S. (1975), "Correlating equations for laminar and turbulent free convection from a vertical plate", *Int. J. Heat Mass Transfer*, Vol. 18, pp. 1323-9.

Gebhart, B. and Pera, L. (1971), "The nature of vertical natural convection flows resulting from the combined buoyancy effects of thermal and mass diffusion", *Int. J. Heat Mass Transfer*, Vol. 14, pp. 2025-50.

Hong, J.T. and Tien, C.L. (1987), "Analysis of thermal dispersion effect on vertical-plate natural convection in porous media", *Int. J. Heat Mass Transfer*, Vol. 30, pp. 143-50.

Hsiao, S.W., Cheng, P. and Chen, C.K. (1992), "Non-uniform porosity and thermal dispersion effects on natural convection about a heated horizontal cylinder in an enclosed porous medium", *Int. J. Heat Mass Transfer*, Vol. 35, pp. 3407-18.

Jang, J.Y. and Chang, W.J. (1988), "Buoyancy-induced inclined boundary layer flow in a porous medium resulting from combined heat and mass buoyancy effects", *Int. Commun. Heat Mass Transfer*, Vol. 15, pp. 17-30.

Johnson, C.H. and Cheng, P. (1978), "Possible similarity solutions for free convection boundary-layers adjacent to flat plates in porous-media", *Int. J. Heat Mass Transfer*, Vol. 21, pp. 709-18.

Kou, H. and Huang, D. (1996), "Some transformation for natural convection on a vertical plate embedded in porous media with prescribed wall temperatures", *Int. Commun. Heat Mass Transfer*, Vol. 23, pp. 273-86.

Lai, F.C. (1991), "Coupled heat and mass transfer by mixed convection from a vertical plate in a saturated porous medium", *Int. Commun. Heat Mass Transfer*, Vol. 18, pp. 93-106.

Lai, F.C. and Kulacki, F.A. (1991), "Non-Darcy mixed convection along a vertical wall in a saturated porous medium", *Int. J. Heat Mass Transfer*, Vol. 113, pp. 252-5.

Pera, L. and Gebhart, B. (1972), "Natural convection boundary layer flow over horizontal and slightly inclined surfaces", *Int. J. Heat Mass Transfer*, Vol. 16, pp. 1131-46.

Plumb, O.A. (1983), "The effect of thermal dispersion on heat transfer in packed bed boundary layers", *Proc. ASME JSME Thermal Engineering Joint Conference*, Vol. 2, pp. 17-22.

Plumb, O.A. and Huenefeld, T.C. (1981), "Non-Darcy natural-convection from heated surfaces in saturated porous-media", *Int. J. Heat Mass Transfer*, Vol. 24, pp. 765-8.

Roblee, L.H.S., Baird, R.M. and Tiernery, J.W. (1958), "Radial porosity variation in packed beds", *A.I.Ch.E. J.*, Vol. 8, pp. 359-61.

Trevisan, O.V. and Bejan, A. (1990), "Mass and heat transfer by natural convection in a vertical slot filled with porous medium", *Int. J. Heat Mass Transfer*, Vol. 29, pp. 403-15.

Vafai, K. and Tien, C.L. (1981), "Boundary and inertia effects on flow and heat transfer in porous media", *Int. J. Heat Mass Transfer*, Vol. 24, pp. 195-203.

Yih, K.A. (1997), "The effect of transpiration on coupled heat and mass transfer in mixed convection over a vertical plate embedded in a saturated porous medium", *Int. Commun. Heat Mass Transfer*, Vol. 24, pp. 265-75.